



CHORUS

This is the accepted manuscript made available via CHORUS. The article has been published as:

Theoretical and experimental determination of L-shell decay rates, line widths, and fluorescence yields in Ge

M. Guerra, J. M. Sampaio, T. I. Madeira, F. Parente, P. Indelicato, J. P. Marques, J. P. Santos, J. Hozowska, J.-Cl. Dousse, L. Loperetti, F. Zeeshan, M. Müller, R. Unterumsberger, and B. Beckhoff

Phys. Rev. A **92**, 022507 — Published 19 August 2015

DOI: [10.1103/PhysRevA.92.022507](https://doi.org/10.1103/PhysRevA.92.022507)

Theoretical and experimental determination of L -shell decay rates, linewidths and fluorescence yields in Ge

M. Guerra^{1,*}, J. M. Sampaio², T. I. Madeira², F. Parente¹, P. Indelicato³, J. P. Marques², J. P. Santos^{1,†}, J. Hosszowska⁴, J.-Cl. Dousse⁴, L. Loperetti⁴, F. Zeeshan⁴, M. Müller⁵, R. Unterumsberger⁵, and B. Beckhoff⁵

¹ *Laboratório de Instrumentação,
Engenharia Biomédica e Física da Radiação (LIBPhys-UNL),
Departamento de Física,
Faculdade de Ciências e Tecnologia,
FCT, Universidade Nova de Lisboa,
2829-516 Caparica, Portugal*

² *BioISI - Biosystems & Integrative Sciences Institute,
Faculdade de Ciências da Universidade de Lisboa,
Campo Grande, C8, 1749-016 Lisboa, Portugal*

³ *Laboratoire Kastler Brossel,
École Normale Supérieure, CNRS,
Sorbonne Universités, UPMC Univ. Paris 06,
Case 74; 4, place Jussieu, 75005 Paris, France*

⁴ *Physics Department, University of Fribourg,
Chemin du Musée 3, CH-1700 Fribourg, Switzerland*

⁵ *Physikalisch-Technische Bundesanstalt (PTB),
Abbestraße 2-12, 10587 Berlin, Germany*

(Dated: July 28, 2015)

Fluorescence yields (FY) for the Ge L -shell were determined by a theoretical and two experimental groups within the framework of the International Initiative on X-ray Fundamental Parameters collaboration. Calculations were performed using the Dirac-Fock method, including relativistic and QED corrections. The experimental value of the L_3 FY ω_{L_3} was determined at the PTB undulator beamline of the synchrotron radiation facility BESSY II in Berlin, Germany, and the $L\alpha_{1,2}$ and $L\beta_1$ linewidths were measured at the Swiss Light Source (SLS), PSI, Switzerland, using monochromatic synchrotron beams and a von Hamos X-ray crystal spectrometer. The measured fluorescence yield and linewidths are compared to the corresponding calculated values.

PACS numbers: 31.30.jf, 32.70.Jz, 32.30.Rj

I. INTRODUCTION

When a hole is created in one of the L -subshells of an atom or ion by a photon or particle collision, the target's electronic structure can suffer a rearrangement through the shifting of electrons from one subshell to another. This process may lead to the emission of an X-ray photon (radiative transition) or to the emission of an electron from an outer shell, carrying the excess energy (radiationless transition, also called Auger emission). In particular, if, in the latter case, the vacancy is filled by an electron from a higher subshell of the same shell, we call it a Coster-Kronig transition [1] or, if, in addition, the emitted electron also belongs to the same shell, a super Coster-Kronig transition.

L -shell radiative transitions are labelled, according to the Siegbahn notation, as $L\alpha$, $L\beta$ and $L\gamma$ transitions, depending on the final-hole shell. In Fig. 1, the transitions that give rise to the L -lines are presented in a schematic

way and the correspondence between the Siegbahn, IU-PAC, and nlj electron configuration (EC) notations is also shown [2, 3]. Following the same reasoning, radiationless transitions are described by identifying the subshells where the initial and final holes lie. For example, the process that involves a transition of the initial hole in the L_1 subshell to the L_3 subshell, with the ejection of a M_4 electron, is identified as L_1 - L_3M_4 transition.

The knowledge of accurate values of decay rates, both for radiative and radiationless transitions is of paramount importance for understanding collision-dynamics and photon-atom or particle-atom interactions, as well as in several applied fields such as X-Ray Fluorescence, Proton Induced X-ray Emission, Auger Electron Spectroscopy, Electron Energy Loss Spectroscopy, and Electron Probe Microanalysis. One of the most important parameters is the fluorescence yield, defined as the relative probability that a hole in a given shell or subshell is filled through a radiative transition. Fluorescence yields are needed in many areas related to physics, namely in quantitative elemental analysis of samples in X-ray spectroscopy to derive the energy-absorption coefficients related to dosimetric quantities, in plasma physics, to characterize the emitted X-ray spectra, and in astrophysics to compute

* mguerra@fct.unl.pt

† jps@fct.unl.pt

approach, with the Breit interaction and the vacuum polarization terms included in the self-consistent field calculation, and other QED effects, such as self-energy and vacuum polarization, included as perturbations [22–25]. A detailed description of the Hamiltonian and wavefunctions can be obtained in [22, 26–28]. The so-called optimized levels (OL) method was used to calculate the wavefunctions and energies of the levels involved in all possible transitions, considering full relaxation of both initial and final states, hence providing more accurate energies and wavefunctions. Since the spin-orbitals of the initial and final levels were optimized separately, they are not orthogonal. To deal with the non-orthogonality of the wavefunctions, the code uses the formalism described by Löwdin [29].

Regarding the radiationless transitions, we have assumed a two-step process, in which the decay is independent from the ionization. Hence, the electron ejected in the process of creation of the initial hole does not interact with the Auger electron, and the core hole state interacts very weakly with the latter electron, allowing for the transition rates to be calculated from perturbation theory. Initial-state wavefunctions were generated for configurations that contain one initial inner-shell vacancy while final state wavefunctions were generated for configurations that contain two higher shell vacancies. Continuum-state wavefunctions were obtained by solving the Dirac-Fock equations with the same atomic potential of the initial state, normalized to represent one ejected electron per unit energy.

In order to keep consistency between the radiative and radiationless calculations, multiconfiguration wavefunctions beyond intermediate coupling were not employed, because the approximation used for the evaluation of the Auger rate cannot be used in an optimized level calculation with correlation orbitals.

B. Decay rates, subshell widths, and fluorescence yields

The width of an atomic level i is given by $\Gamma_i = \hbar \sum_j W_{ij}$, where W_{ij} is the transition probability from level i to all possible final levels j , including contributions from radiative and radiationless processes, and is given by the sum of the radiative Γ_R , Auger Γ_A , and Coster-Kronig Γ_{CK} , widths.

If the system has no unpaired outer electrons, or if the interaction between the hole and those electrons is neglected, to each one-hole configuration corresponds only one level. Therefore the width of the configuration is just the width of the corresponding level.

The situation is more complicated, in general, if the interaction with existing unpaired electrons is taken in account. The fine structure resulting from the interaction between the inner-hole and these electrons leads to a number of different levels for a given configuration, each one identified by a particular value of the total angular

momentum J and by the electronic coupling. This is the case of Ge, where two p electrons exist in the outermost shell.

Assuming that the initial one hole S_n -subshell multiplet levels, identified by the total angular momentum J_i and the coupling scheme, are statistically populated (in the experiments carried in this work there is no preferential population of any given magnetic sublevel), the radiative (R) width of a subshell S_n is obtained by summing the partial widths, $\Gamma_{i,j}^R$, for all levels i of the system with one hole in subshell S_n decaying radiatively to all levels j of the system with one hole in a higher subshell,

$$\Gamma_{S_n}^R = \frac{\sum_i \sum_j (2J_i + 1) \Gamma_{i,j}^R}{\sum_i (2J_i + 1)}, \quad (1)$$

Here,

$$\Gamma_{i,j}^R = \hbar W_{i,j}^R, \quad (2)$$

In the same way, the radiationless width of the subshell S_n is given by

$$\Gamma_{S_n}^{\text{NR}} = \frac{\sum_i \sum_j (2J_i + 1) \Gamma_{i,k}^{\text{NR}}}{\sum_i (2J_i + 1)}, \quad (3)$$

where

$$\Gamma_{i,k}^{\text{NR}} = \hbar W_{i,k}^{\text{NR}}. \quad (4)$$

Here $W_{i,k}^{\text{NR}}$ is the radiationless transition probability from level i to level k . Thus, $\Gamma_{i,k}^{\text{NR}}$ is the partial width corresponding to the radiationless transition from the level i in the system with one hole in subshell S_n to the level k of the system with two holes in higher shells or subshells, with the emission of an electron to the continuum.

Henceforth, the index i will be related to the configuration S_n and spans over all possible initial levels (with different total angular momentum, J_i). Final levels of the system, with one or two holes, corresponding to radiative and radiationless transitions, respectively, will be denoted by the indexes j or k .

Radiationless widths include contributions from Auger, Coster-Kronig, and super-Coster-Kronig transitions. In the Auger contributions, the original hole is filled by an electron from a higher shell and a second electron is emitted also from a higher shell; in the Coster-Kronig contributions, the initial hole in level is filled with by electron from the same shell and the emitted electron belongs to a higher shell or to another subshell of the same shell. The latter are also called super-Coster-Kronig transitions. Thus, the (total) width of a S_n shell is

$$\Gamma_{S_n} = \Gamma_{S_n}^R + \Gamma_{S_n}^{\text{NR}}. \quad (5)$$

TABLE I. Calculated width, in eV, of the L_1 , L_2 , L_3 , M_1 , M_2 , M_3 , M_4 and M_5 one-hole configurations.

	L_1	L_2	L_3	M_1	M_2	M_3	M_4	M_5
This work (Theo.)	6.11	0.94	0.98	2.19	3.26	2.98	0.013	0.012
EADL [31]	8.71	0.84	0.84	4.13	3.99	3.71	0.05	0.044
Campbell [30]	3.8	0.86	0.86	2.1	2.3	2.3	0.05	0.044

The widths of the Ge L - and M -subshells, computed in this work using this equation are listed in Table I together with the recommended values Campbell and Papp [30], and the EADL values [31].

The FY of an atomic subshell is defined as the probability that the vacancy in that subshell is filled through a radiative transition, and, if we neglect other less probable modes of decay, such as two photon transitions, hyperfine quenchings, etc..., is given by

$$\omega_{S_n} = \frac{\Gamma_{S_n}^R}{\Gamma_{S_n}^R + \Gamma_{S_n}^{\text{NR}}}, \quad (6)$$

where for the L -shell, the index $n = 1, 2, 3$ denote holes in the orbitals $2s_{1/2}$, $2p_{1/2}$, and $2p_{3/2}$.

Assuming that the initial L -subshell multiplet levels, identified by the total angular momentum J_i , are statistically populated, and considering the relation between the natural widths and the decay rates, Eq. (6) may be written as

$$\omega_{L_n} = \frac{\sum_i \sum_j (2J_i + 1) W_{i,j}^R}{\sum_i (2J_i + 1) \left(\sum_j W_{i,j}^R + \sum_k W_{i,k}^{\text{NR}} \right)}, \quad (7)$$

where $W_{i,j}^R$ and $W_{i,k}^{\text{NR}}$ stand for the radiative and radiationless decay rates, respectively, of the initial one-hole level i in the L_n -subshell to a one-hole level j or to a two-hole level k . Similarly to the fluorescence yield, the Auger a_{L_n} yield for the L -subshells is defined as

$$a_{L_n} = \frac{\sum_{i,k} (2J_i + 1) (W_{i,k}^{\text{NR}})}{\sum_i (2J_i + 1) \left(\sum_j W_{i,j}^R + \sum_k W_{i,k}^{\text{NR}} \right)}, \quad (8)$$

where the k index refers to levels with two holes in M , N or shells higher shells. On the other hand, the Coster-Kronig $f_{L_n, L_{n'}}$ yields for the L -subshells are given by an identical expression

$$f_{L_n, L_{n'}} = \frac{\sum_{i,k'} (2J_i + 1) (W_{i,k'}^{\text{NR}})}{\sum_i (2J_i + 1) \left(\sum_j W_{i,j}^R + \sum_{k'} W_{i,k'}^{\text{NR}} \right)}, \quad (9)$$

but, in this equation the k' index refers to levels with one hole in a subshell L'_n ($n < n'$) and a second hole in a higher shell.

From these definitions, one can conclude that the following relation is valid for each subshell L_n :

$$\omega_{L_n} + a_{L_n} + \sum_{n' > n} f_{L_n, L_{n'}} = 1. \quad (10)$$

C. Linewidths

The theoretical width of a line corresponding to the radiative transition between two atomic levels is the sum of the widths of the two levels involved. As referred above, when no unpaired outer electrons exist, or the interaction between the hole and those electrons is neglected, to each one-hole configuration corresponds just one level. In these cases the width of the one line corresponding to the transition between two one-hole configurations is just the sum of the widths of the initial and final level. However, in most cases, unpaired outer electrons exist and a given number of levels correspond to the initial and final configurations, leading to a set of individual component lines. This is the case of Ge, where two unpaired $4p$ electrons exist. Nevertheless, we calculated the $L\alpha_1$, $L\alpha_2$, and $L\beta_1$ linewidths by adding the widths of the L_3 and M_5 , L_3 and M_4 , and L_2 and M_4 subshells, respectively. The results are listed in Table II.

The component lines referred above are usually spread in energy, leading to an enlargement of the observable width. One remarkable example is the width of the $K\alpha_{1,2}$ line for low- and medium- Z atoms [15], whose comparison to experimental values has to be performed very carefully for this exact reason.

In Ge, the $L\alpha_{1,2}$ line manifold is made up of a set of a large number of lines corresponding to transitions between initial and final fine structure atomic levels belonging, respectively, to a configuration with one hole in the L_3 subshell and configurations with one hole in the M_4 and M_5 subshells, respectively. The two sets of lines are spread in energy and superimposed, making impossible a clear separation of the $L\alpha_1$ and $L\alpha_2$ "lines", as seen in Fig. 2. We obtained the width of all individual levels in the initial and final one-hole configurations by calculating the radiative and radiationless transition probabilities from each of those levels to all possible final levels. In order to compare the theoretical results to the experimental spectrum, one has to include the experimental resolution on the synthesized spectrum. This, however is not straightforward, since the experimental broadening is obtained from a one or two component fit to the Mg $K\alpha_1$ and Se $L\alpha_1$ lines (see Section III), whereas for the Se $L\alpha_{1,2}$ we find the same overlapping between the two lines as in Ge. Thus, the inclusion of the experimental broadening in the synthesized spectrum can only be correctly performed if one assumes a two component line for the Ge $L\alpha_{1,2}$ manifold. With this in mind we have calculated the energy centroid of the $L\alpha_1$ and $L\alpha_2$ lines through a line intensity weighted average of the individual level energies. Due to the Lorentzian profile of the experimental

TABLE II. Measured and calculated widths of the L_{α_1} , L_{α_2} , $L_{\alpha_{1,2}}$ and L_{β_1} lines in eV. The notation 0.933(62/17) means 0.933 ± 0.062 eV with an included statistical error of 0.017 eV. The SR beam energy is in keV. The experimental $L_{\alpha_{1,2}}$ widths were obtained from fits with a single Lorentzian function of the experimental data. The theoretical widths of the L_{α_1} and L_{α_2} lines were calculated by summing the initial and final subshell widths, while the $L_{\alpha_{1,2}}$ width corresponds to the FWHM of the $L_{\alpha_{1,2}}$ synthesized spectrum (Fig 3) minus the experimental broadening.

	SR beam energy (keV)	L_{α_1}	L_{α_2}	$L_{\alpha_{1,2}}$	L_{β_1}
This Work (Theo.)		0.988	0.992	0.928	0.954
EADL [31]		0.884	0.890		0.890
Campbell [30]		0.904	0.910		0.905
This Work (Expt.)	1.23			0.811(60/8)	–
	1.30			0.875(60/8)	0.933(62/17)
	1.45			0.859(60/6)	0.955(62/24)

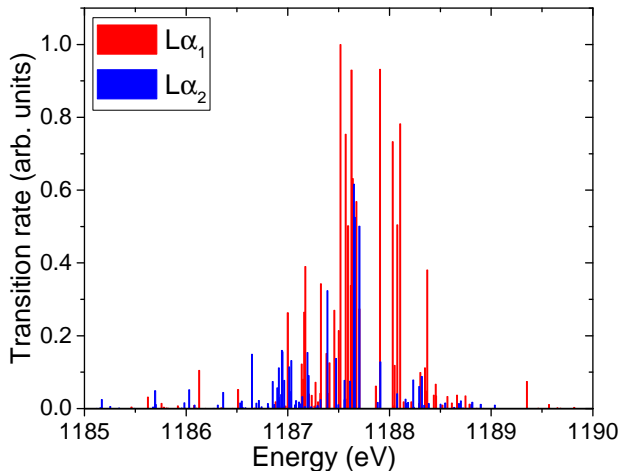


FIG. 2. Normalized calculated transition rates in the Ge $L_{\alpha_{1,2}}$ line manifold.

broadening, we have adopted a Lorentzian distribution for each of the two resulting lines, whose width is given by our theoretical results of Table II plus the experimental broadening of 0.63 eV. The obtained normalized profile is shown together with the experimental values, at a beam energy of 1.23 keV, in Fig. 3.

III. EXPERIMENT

A. Fluorescence yields

The FY of the Ge L_3 subshell has been determined by means of reference-free X-ray fluorescence spectrometry [19] using very thin free-standing foils as specimens with well-known composition. This approach is described in several recent publications [33–36] and we will provide only a brief description in the following. A free-standing Ge foil with a nominal thickness of 300 nm and 99.99 % purity has been used for the experiments, which have been carried out at PTB’s plane grating monochromator beamline for undulator radiation at the synchrotron radiation facility BESSY II [37]. The Ge foil was irradiated with a monochromatic X-ray beam under an angle of in-

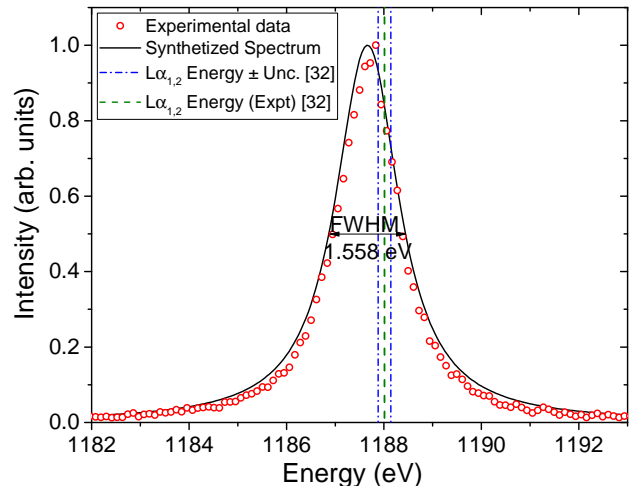


FIG. 3. Ge $L_{\alpha_{1,2}}$ synthesized spectrum compared to experimental data at a beam energy of 1.23 keV. Presented are also the combined $L_{\alpha_{1,2}}$ experimental energy value of Deslattes *et al.* [32].

cidence γ_1 of 45° . Three photon energies E_0 between the Ge L_3 and L_2 subshell absorption edges (1220 eV, 1225 eV, and 1231 eV) were used to excite the specimen and the incident photon flux I_0 was recorded with a radiometrically calibrated photo diode [38]. An energy-dispersive Silicon-Drift detector (SDD), which was calibrated with respect to both the detection efficiency $\epsilon_{\text{set}}(E_{X_i})$ and the response behavior [39], was positioned at an observation angle γ_2 of 45° . In front of the SDD detector a calibrated diaphragm was placed at a well-known distance in order to define accurately the solid angle $d\Omega$ of detection. Using this detector, the fluorescence radiation emitted by the Ge foil in the solid angle defined by the diaphragm was measured. In addition, transmission measurements in a wide energy range below and above the L_3 absorption edge, including the three selected excitation energies as well as at the two fluorescence line energies of interest, have been performed. From the transmission I_{tr}/I_0 of the Ge foil the product of the Ge mass absorption cross section μ_E , the density ρ , and the thickness d of the foil could be derived directly without using any database val-

ues for the absorption cross sections. The detected count rate N_i of the line the fluorescence radiation of line i (L_α or L_l) having the photon energy E_i is

$$N_i = I_0 \frac{d\Omega}{4\pi} \epsilon_{\text{det}}(E_i) M_i(E_0) \frac{\rho d}{\sin(\gamma_1)} \tau_{E_0} \omega_{L_3} g_i, \quad (11)$$

$$M_i(E_0) = \frac{1}{\rho d \mu_{E_0} / \sin(\gamma_1) + \rho d \mu_{E_i} / \sin(\gamma_2)} \left(1 - e^{\rho d \mu_{E_0} / \sin(\gamma_1) + \rho d \mu_{E_i} / \sin(\gamma_2)} \right) \quad (12)$$

is the absorption correction factor derived from transmission measurements, and ω_{L_3} is the FY of the L_3 subshell to be determined, g_i is the probability of emission of the line i (L_α or L_l), and τ_{E_0} is the photoelectric cross section for Ge.

Using the fact that the scattering cross sections of Ge for the low photon energies involved here are only about 0.1 % of the mass absorption cross section μ_{E_0} , the photoelectric cross section τ_{E_0} can be approximated very well by the L_3 contribution of μ_{E_0} . The L_3 contribution of μ_{E_0} can be obtained by extrapolating the higher-shell photoelectric cross section contributions $\mu_{M,N}$, the energy dependence of which can be derived below the L_3 edge, to the excitation energies above the L_3 edge. Using the transmission measurements, the term $\rho d / \sin(\gamma_1) \tau_{E_0}$ can be substituted by $[\log(I_{\text{tr}}/I_0) - u_{M,N,E_0}]$ [34].

The transition probability g_i for both the L_α and the L_l lines can be derived from the detected count rates of both lines when corrected for both the detector efficiency and the absorption effects. Values of 0.950 ± 0.002 and 0.050 ± 0.002 were determined for g_{L_α} and g_{L_l} , respectively. At this point all parameters in Eq.(11) except the FY ω_{L_3} are known from the instrumental calibration and experimental determinations. The FY of the Ge L_3 subshell can now be derived without using any parameters from databases with frequently unknown uncertainties. We derived a value of $(1.20 \pm 0.11) \times 10^{-2}$ for the FY of the Ge L_3 subshell. The standard deviation of the FY derived at three different excitation energies between L_3 and L_2 is 0.04×10^{-2} and originates mainly from the uncertainty of the spectral deconvolution, which was used to derive the detected count rates of the fluorescence lines. The other main contributions to the total relative uncertainty of 9.2 % are caused by the determination of the absorption correction factor (5 %) and the extrapolation of M and N shell contributions to μ_{E_0} (about 21 %) above the L_3 absorption edge (6 %). Future works at PTB will aim at the completion of subshell fundamental parameters such as photoionization cross sections, fluorescence yields and Coster-Kronig factors using a calibrated wavelength-dispersive grating spectrometer [40].

where

B. Linewidths

The linewidth measurements were carried out at the Swiss Light Source (SLS) of the Paul Scherrer Institute (PSI), in Villigen, Switzerland, using the von Hamos Bragg-type bent crystal spectrometer of the University of Fribourg [41]. The spectrometer was installed at the beam line PHOENIX, downstream from the experimental chamber of the endstation I. The synchrotron radiation from the elliptical undulator was monochromatized with a Beryl(1-10) double crystal monochromator. Upper harmonics were suppressed with dedicated mirrors. To probe the possible broadening of the $L\alpha_{1,2}$ and $L\beta_1$ lines of interest by partly overlapping M -satellites originating from $L_{1,2} - L_3M$ and $L_1 - L_2M$ Coster-Kronig (CK) transitions, respectively, the measurements were performed at 1.23 keV (i.e., between the Ge L_3 and L_2 edges), 1.3 keV (between the L_2 and L_1 edges) and at 1.45 keV (above the L_1 edge). For each beam energy the bandwidth was about 0.5 eV. The beam spot on the sample was 0.5 mm wide and 2.6 mm high and the flux was 5×10^{10} - 10^{11} photons/s. The sample consisted of a 0.6 mm thick Ge crystal wafer.

The spectrometer was operated in the slitless geometry and the fluorescence from the sample was measured at grazing emission angles so that the contribution of the apparent source width to the energy resolution of the spectrometer was negligibly small. For the diffraction of the fluorescence X-rays, a 80 mm high \times 20 mm wide \times 100 μm thick Beryl(1-10) crystal, bent cylindrically to a radius of 25.4 cm, was employed. The diffracted X-rays were collected with a 26 mm long \times 8 mm high back-illuminated CCD x-ray camera having a spatial resolution of 20 μm .

For the energy calibration of the spectrometer, the $K\alpha$ transition of Mg was measured and the energy of 1253.688(11) eV reported in [42] was assigned to the fitted centroid position of the $K\alpha_1$ line. This transition as well as the $L\alpha_1$ line of Se ($E = 1379.10$ eV) were also used to determine the instrumental response. It was found that the instrumental response of the von Hamos spectrometer operated in the slitless geometry could be well reproduced by a Lorentzian profile. The energy-dependent width of the latter was determined by subtracting the natural widths of the two transitions from

the total transition widths obtained from the fitting procedure. The natural widths of the Mg $K\alpha_1$ and Se $L\alpha_1$ X-ray lines were derived from the atomic level widths reported by Campbell and Papp [30]. Interpolating the so-obtained values for the energies corresponding to the $L\alpha_{1,2}$ and $L\beta_1$ transitions of Ge, instrumental FWHM broadenings of 0.63(3) eV and 0.61(3) eV, respectively, were found.

For illustration, the Ge L X-ray spectra measured at 1.23 keV (top panel), 1.30 keV (middle panel) and 1.45 keV (bottom panel) are depicted in Fig. 4. In the top panel the $L\beta_1$ line and the M satellites of the $L\alpha_{1,2}$ lines are not observed since the beam energy in this case was lower than the energy of the L_2 edge. In the mid panel (beam energy tuned between the L_2 and L_1 edges), some weak satellite structure (relative intensity of 3.3%) due to $L_2 - L_3M$ CK transitions is visible for the $L\alpha_{1,2}$ transitions but not for the $L\beta_1$ one. In the bottom panel which corresponds to a beam energy lying above the L_1 edge, a rich satellite structure (relative intensity of 21.3%) due mainly to $L_1 - L_3M$ CK transitions is observed for the $L\alpha_{1,2}$ lines while some weaker M satellites (relative intensity of 9.4%), due to $L_1 - L_2M$ CK transitions, are also visible on the high energy side of the $L\beta_1$ line. However, thanks to the high resolving power of the spectrometer, the M satellites could be well separated from their parent diagram lines and no significant broadening of the $L\alpha_{1,2}$ and $L\beta_1$ lines as a function of the beam energy was observed (see Table II).

IV. RESULTS AND DISCUSSION

A. Linewidths and decay rates

In Table I we list the level widths for the L - and M -shells of Ge calculated in this work. They are compared to the corresponding EADL [31] atomic level widths and the values from Campbell and Papp [30]. The EADL database relies mostly on Dirac-Hartree-Slater calculations of Chen and Scofield. It is well known that this method seriously overpredicts the strength of Coster-Kronig transitions, resulting in erroneous fluorescent yields and widths. The database results are then normalized with the use of a Z dependence scaling for the fluorescence yield, in which we encounter the familiar Z^4 dependence for the radiative yield. This approach is quite different from ours, as the calculations are performed with a Dirac-Fock approach, in which both radiative and nonradiative are obtained in the same frame-set. Table II shows the theoretical linewidths for the $L\alpha_1$ and $L\alpha_2$ lines, and both the theoretical and experimental linewidths for the $L\alpha_{1,2}$ and $L\beta_1$ lines obtained in this work as well as the linewidths of the two transitions derived from the EADL [31] atomic level widths and from the values recommended by Campbell and Papp [30]. As it can be seen, there is a very good agreement between the calculated and measured value of the $L\beta_1$ linewidth,

less than 2%, well inside the one sigma interval. For the $L\alpha_{1,2}$ line, however, we find a discrepancy between the theoretical predictions and the experimental values of about 10%. Note, that because the $L\alpha_{1,2}$ line is composed of a manifold of superimposed $L\alpha_1$ and $L\alpha_2$ transitions a direct comparison between the measured and calculated $L\alpha_1$ and $L\alpha_2$ linewidths is not possible when only two Lorentzian functions are used to fit the experimental spectrum as shown in Fig. 4. Therefore, for a meaningful comparison, the FWHM of the experimental and synthesized $L\alpha_{1,2}$ spectrum was considered. To extract the FWHM values for the $L\alpha_{1,2}$ doublet the experimental spectra for the three beam energies were fitted with a single Lorentzian and an experimental broadening of 0.63 eV was subtracted. An average natural linewidth of 0.848(60) eV was found, which lies about 10% below the theoretical value shown in Table II.

Finally, as it can be seen in II, a tiny change of the width with the beam energy is observed. The change is hardly significant in view of the quoted uncertainties (± 0.060 eV). Nevertheless, it seems that there is a trend for a slight increase of the width with growing beam energy. This increase can be explained by unresolved N-satellites resulting from N-shell shake processes following the creation by photoionization of the primary L_3 hole and also, for the highest beam energy, by L_1L_3N and L_2L_3N CK transitions which lead to $L_3^{-1}N^{-1}$ double vacancy states.

In Table III, we present the computed radiative decay rates (in a.u.) for Ge. The shown values represent the sums, for all final one-hole levels for each one-hole initial configuration, arranged by their initial total angular momentum, J_i . The statistical weight of each initial level is taken into account in the final results. These decay rates include the sum over all possible electric and magnetic multipoles. The first column identifies the initial and final one-hole configurations: For example, $L_2 - M_4$ means that a hole from the L_2 subshell moves to the M_4 subshell emitting a photon in the process. The final column presents the contribution of each final subshell to the total radiative decay rate of the initial subshell.

The theoretical radiationless transition probability values for the L -shell of Ge are presented in Table IV. In this table, the values in each cell represent the sum over the final two-hole levels, for a fixed initial one-hole configuration with a given initial total angular momentum, J_i , and fixing one of the two resulting final holes. The values shown also include the statistical weight factor ($2J_i + 1$). The notation used in the first column reflects these sums: for instance, the $L_1 - L_2 - L_{2,3}M_{1\dots 5}N_{1,2}$ line means that an initial configuration with a hole in the L_1 subshell decays to a final state with one hole in the L_2 subshell and a second hole in either the $L_{2,3}$, $M_{1\dots 5}$ or $N_{1,2}$ subshells.

In the final column we list, as a percentage of the total, the contribution of each group to the total decay rates. We conclude that the contribution of the Coster-Kronig transitions in the L_1 one-hole initial configuration is about 89 %, i.e., the computational effort to calculate

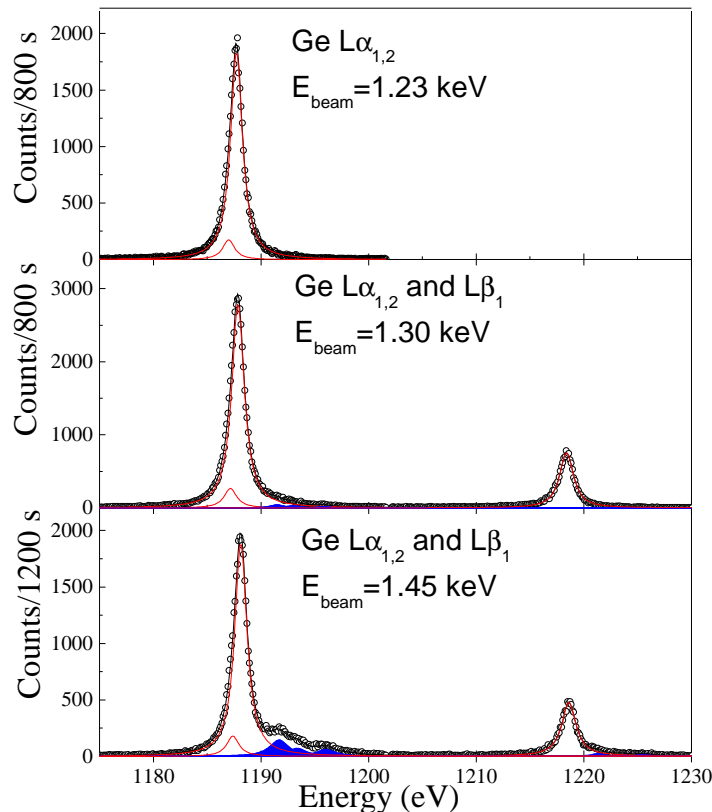


FIG. 4. (color online) High energy resolution $L\alpha_{1,2}$ ($L_3 - M_{5,4}$ transition) and $L\beta_1$ ($L_2 - M_4$ transition) x-ray spectra of a 0.6 mm thick crystalline Ge wafer irradiated with monochromatic synchrotron radiation of different energies. The red curves correspond to the fits of the $L\alpha_2$ (weakest bump), $L\alpha_1$ and $L\beta_1$ diagram lines, the filled blue areas to the M -shell satellites induced by CK transitions. In the fit the same width was assumed for the two components of the doublet, and the energy separation of the $L\alpha_2$ and $L\alpha_1$ lines was fixed at 0.75 eV according to the theoretical transition energies reported in [42]. The fit yields 0.13(1) for the intensity ratio of the $L\alpha_2$ to $L\alpha_1$ transitions.

the other contributions represent less than 11 % of the total value. Regarding the initial configurations with one hole in the L_2 and L_3 subshells, the contributions are much more spread out through all the final two-hole levels.

B. Fluorescence yields

The theoretical fluorescence yields ω_{L_1} , ω_{L_2} and ω_{L_3} were derived from Eq. (7) from the radiative and radiationless rates presented in the previous subsection. The obtained results ($\omega_{L_1} = 0.00149$, $\omega_{L_2} = 0.0151$ and $\omega_{L_3} = 0.0136$) are listed in Table V together with the experimental value of ω_{L_3} determined in this work and with the theoretical values obtained by other authors. Regarding the ω_{L_1} , ω_{L_2} fluorescence yields, they have not been determined experimentally yet. For the ω_{L_3} FY, a discrepancy of about 12% between the calculated and measured value is found. However, comparing the results to other authors, we find a less than 1% difference with the RDHS value of Puri [43], recommended

by Campbell [44] in his compilation, a 10% discrepancy with the result from Krause [45] and a 5% shift regarding the calculated value of McGuire [46]. On the other hand, the comparison with the theoretical results of the L_1 and L_2 subshells from the other authors raises some questions. For instance, the results from Chen *et al.* [47] and McGuire *et al.* [46] reveal a discrepancy with our results of almost 50%. Comparing with the results of Krause, we see a 61% deviation for the L_1 subshell and 14% for L_2 .

V. CONCLUSIONS

In this work, we have presented the results of a collaboration between experimental and theoretical groups, within the International Initiative on X-ray Fundamental Parameters framework, to obtain decay rates and fluorescence yields for Ge. The Dirac-Fock method, including relativistic and QED corrections, has been used to obtain the wavefunctions and binding energy values, as well as, L -shell radiative and radiationless decay rates for Ge.

TABLE III. Ge L -shell radiative decay rates for each value of total angular momentum J_i of the initial configuration (in a.u.). The total value for each final configuration, and for each value of J_i , takes into account the statistical weight of each initial level i .

	$J_i = 1/2$	$J_i = 3/2$	$J_i = 5/2$	$J_i = 7/2$	Total	%
L_1-L_1	6.50×10^{-16}	7.48×10^{-17}	1.17×10^{-16}		8.42×10^{-16}	<0.001
L_1-L_2	1.12×10^{-05}	1.48×10^{-05}	1.76×10^{-05}		4.37×10^{-05}	0.436
L_1-L_3	2.97×10^{-05}	5.97×10^{-05}	5.98×10^{-05}		1.49×10^{-04}	1.486
L_1-M_1	3.22×10^{-07}	4.36×10^{-07}	5.02×10^{-07}		1.26×10^{-06}	0.013
L_1-M_2	6.64×10^{-04}	1.37×10^{-03}	1.33×10^{-03}		3.36×10^{-03}	33.445
L_1-M_3	1.21×10^{-03}	2.48×10^{-03}	2.53×10^{-03}		6.21×10^{-03}	61.851
L_1-M_4	3.13×10^{-06}	9.02×10^{-06}	3.88×10^{-06}		1.60×10^{-05}	0.160
L_1-M_5	4.81×10^{-06}	6.93×10^{-06}	1.22×10^{-05}		2.39×10^{-05}	0.238
L_1-N_1	7.47×10^{-08}	1.01×10^{-07}	1.12×10^{-07}		2.87×10^{-07}	0.003
L_1-N_2	6.37×10^{-05}	1.26×10^{-04}	4.85×10^{-05}		2.38×10^{-04}	2.369
Total	1.98×10^{-03}	4.06×10^{-03}	4.00×10^{-03}		1.00×10^{-02}	
L_2-L_2	1.78×10^{-15}	1.26×10^{-15}	1.66×10^{-16}		3.20×10^{-15}	<0.001
L_2-L_3	4.03×10^{-11}	8.32×10^{-11}	8.32×10^{-11}		2.07×10^{-10}	<0.001
L_2-M_1	1.37×10^{-04}	2.67×10^{-04}	2.60×10^{-04}		6.65×10^{-04}	4.250
L_2-M_2	3.64×10^{-07}	4.19×10^{-07}	5.82×10^{-07}		1.37×10^{-06}	0.009
L_2-M_3	5.14×10^{-07}	9.88×10^{-07}	8.79×10^{-07}		2.38×10^{-06}	0.015
L_2-M_4	2.38×10^{-03}	4.74×10^{-03}	4.38×10^{-03}		1.15×10^{-02}	73.507
L_2-M_5	5.74×10^{-04}	1.00×10^{-03}	1.27×10^{-03}		2.84×10^{-03}	18.171
L_2-N_1	5.21×10^{-04}	8.54×10^{-05}	1.59×10^{-05}		6.23×10^{-04}	3.982
L_2-N_2	8.19×10^{-06}	1.47×10^{-06}	1.74×10^{-08}		9.67×10^{-06}	0.062
Total	3.62×10^{-03}	6.09×10^{-03}	5.93×10^{-03}		1.56×10^{-02}	
L_3-L_3	1.19×10^{-16}	2.06×10^{-15}	1.54×10^{-16}	1.46×10^{-16}	2.48×10^{-15}	<0.001
L_3-M_1	1.43×10^{-04}	4.67×10^{-04}	4.16×10^{-04}	3.70×10^{-04}	1.40×10^{-03}	4.771
L_3-M_2	2.47×10^{-07}	8.59×10^{-07}	6.64×10^{-07}	7.87×10^{-07}	2.56×10^{-06}	0.009
L_3-M_3	3.14×10^{-07}	1.72×10^{-06}	1.43×10^{-06}	1.07×10^{-06}	4.53×10^{-06}	0.015
L_3-M_4	1.08×10^{-03}	1.94×10^{-03}	2.15×10^{-03}	2.44×10^{-04}	5.42×10^{-03}	18.517
L_3-M_5	1.71×10^{-03}	7.35×10^{-03}	6.11×10^{-03}	7.13×10^{-03}	2.23×10^{-02}	76.247
L_3-N_1	2.86×10^{-05}	5.16×10^{-05}	2.55×10^{-05}	2.29×10^{-05}	1.29×10^{-04}	0.439
L_3-N_2	5.23×10^{-07}	6.99×10^{-07}	1.48×10^{-08}	1.20×10^{-08}	1.25×10^{-06}	0.004
Total	2.96×10^{-03}	9.81×10^{-03}	8.71×10^{-03}	7.76×10^{-03}	2.92×10^{-02}	

TABLE IV. L -shell radiationless decay rates for Ge as a function of the initial state total angular momentum J_i (in a.u.). $L_1 - L_2 - L_{2,3}M_{1\dots 5}N_{1,2}$ means that after the radiationless transition the atom with an initial L_1 -subshell vacancy ends up with a vacancy in the L_2 subshell and another vacancy in either of the $L_{2,3}$, $M_{1\dots 5}$, and $N_{1,2}$ shells. The total value for each final state shell, and for each J_i , takes into account the statistical weight of each J_i .

	$J_i = 1/2$	$J_i = 3/2$	$J_i = 5/2$	$J_i = 7/2$	Total	%
$L_1-L_2-L_{2,3}M_{1\dots 5}N_{1,2}$	3.48×10^{-01}	7.13×10^{-01}	7.52×10^{-01}		$1.81 \times 10^{+00}$	27.003
$L_1-L_3-L_3M_{1\dots 5}N_{1,2}$	8.70×10^{-01}	$1.64 \times 10^{+00}$	$1.68 \times 10^{+00}$		$4.18 \times 10^{+00}$	62.271
$L_1-M_1-M_{1\dots 5}N_{1,2}$	8.98×10^{-02}	1.80×10^{-01}	1.80×10^{-01}		4.50×10^{-01}	6.704
$L_1-M_2-M_{2\dots 5}N_{1,2}$	1.68×10^{-02}	3.39×10^{-02}	3.47×10^{-02}		8.53×10^{-02}	1.271
$L_1-M_3-M_{3\dots 5}N_{1,2}$	2.45×10^{-03}	4.75×10^{-03}	4.07×10^{-03}		1.13×10^{-02}	0.168
$L_1-M_4-M_{4,5}N_{1,2}$	3.09×10^{-02}	6.19×10^{-02}	6.25×10^{-02}		1.55×10^{-01}	2.310
$L_1-M_5-M_5N_{1,2}$	3.70×10^{-03}	7.32×10^{-03}	6.83×10^{-03}		1.78×10^{-02}	0.266
$L_1-N_1-N_{1,2}$	8.39×10^{-05}	1.68×10^{-04}	1.82×10^{-04}		4.34×10^{-04}	0.006
$L_1-N_2-N_2$	1.67×10^{-07}	2.17×10^{-07}	4.01×10^{-07}		7.86×10^{-07}	< 0.001
Total	$1.36 \times 10^{+00}$	$2.64 \times 10^{+00}$	$2.72 \times 10^{+00}$		$6.72 \times 10^{+00}$	
$L_2-L_3-L_3M_{1\dots 5}N_{1,2}$	2.48×10^{-03}	5.00×10^{-03}	4.92×10^{-03}		1.24×10^{-02}	1.216
$L_2-M_1-M_{1\dots 5}N_{1,2}$	1.56×10^{-02}	3.12×10^{-02}	3.07×10^{-02}		7.75×10^{-02}	7.599
$L_2-M_2-M_{2\dots 5}N_{1,2}$	8.79×10^{-02}	1.96×10^{-01}	1.95×10^{-01}		4.78×10^{-01}	46.916
$L_2-M_3-M_{3\dots 5}N_{1,2}$	2.19×10^{-02}	2.86×10^{-02}	2.89×10^{-02}		7.94×10^{-02}	7.789
$L_2-M_4-M_{4,5}N_{1,2}$	4.61×10^{-02}	1.20×10^{-01}	1.22×10^{-01}		2.88×10^{-01}	28.223
$L_2-M_5-M_5N_{1,2}$	2.81×10^{-02}	2.95×10^{-02}	2.65×10^{-02}		8.41×10^{-02}	8.248
$L_2-N_1-N_{1,2}$	1.87×10^{-05}	3.82×10^{-05}	5.38×10^{-06}		6.23×10^{-05}	0.006
$L_2-N_2-N_2$	9.92×10^{-06}	1.83×10^{-05}	1.40×10^{-06}		2.96×10^{-05}	0.003
Total	2.02×10^{-01}	4.10×10^{-01}	4.08×10^{-01}		$1.02 \times 10^{+00}$	
$L_3-M_1-M_{1\dots 5}N_{1,2}$	1.63×10^{-02}	5.36×10^{-02}	4.75×10^{-02}	4.21×10^{-02}	1.59×10^{-01}	7.508
$L_3-M_2-M_{2\dots 5}C_{1,2}$	6.45×10^{-02}	2.17×10^{-01}	1.83×10^{-01}	1.65×10^{-01}	6.29×10^{-01}	29.621
$L_3-M_3-M_{3\dots 5}N_{1,2}$	5.23×10^{-02}	1.72×10^{-01}	1.63×10^{-01}	1.40×10^{-01}	5.27×10^{-01}	24.806
$L_3-M_4-M_{4,5}N_{1,2}$	5.93×10^{-02}	2.05×10^{-01}	1.88×10^{-01}	1.67×10^{-01}	6.19×10^{-01}	29.137
$L_3-M_5-M_5N_{1,2}$	2.24×10^{-02}	6.52×10^{-02}	5.39×10^{-02}	4.80×10^{-02}	1.89×10^{-01}	8.918
$L_3-N_1-N_{1,2}$	3.97×10^{-05}	7.09×10^{-05}	9.41×10^{-06}	3.09×10^{-06}	1.23×10^{-04}	0.006
$L_3-N_2-N_2$	2.12×10^{-05}	3.24×10^{-05}	4.43×10^{-07}	2.93×10^{-06}	5.69×10^{-05}	0.003
Total	2.15×10^{-01}	7.13×10^{-01}	6.35×10^{-01}	5.62×10^{-01}	$2.12 \times 10^{+00}$	

This approach leads to FY values of 0.00149, 0.0151 and 0.136 for the L_1 , L_2 and L_3 subshells, respectively. We have estimated the uncertainty of the fluorescence yield to be 3%, by error propagation of Eq. 6. The individual uncertainty of the partial width $\Gamma_{S_n}^R$, was calculated as an average of the transition rates differences between the length and velocity gauge, weighted by the transition rates themselves. Due to the impossibility of using the same procedure for Auger rates, but having in mind that the quality of the wavefunctions should be similar for two-hole states, we have adopted for the uncertainty of $\Gamma_{S_n}^{NR}$ the same value as the uncertainty of $\Gamma_{S_n}^R$. This led to final uncertainties of the fluorescence yields for L_1 , L_2 and L_3 subshells, lower than 3%.

The experimental value of $\omega_{L_3} = 0.0120$, with an uncertainty of 9.2%, was determined at the PTB undulator beamline at the synchrotron radiation facility BESSY II in Berlin, Germany, employing calibrated instrumentation. The linewidths of the $L\alpha_{1,2}$ and $L\beta_1$ were measured at the Swiss Light Source (SLS), PSI, Switzerland, using monochromatic synchrotron beams and a von Hamos crystal spectrometer. The measured FY and linewidths were compared to the corresponding calculated values. We consider that this combined theoretical and experimental work in X-ray fundamental parameters has to be extended to other elements and shells in order to bench-

mark the theoretical methods employed here.

ACKNOWLEDGMENTS

This research was supported in part by Fundação para a Ciência e a Tecnologia (FCT), Portugal, through the projects No. PEstOE/FIS/UI0303/2011 and No. PTDC/FIS/117606/2010, financed by the European Community Fund FEDER through the COMPETE. We also thank the Allianz Program of the Helmholtz Association, contract No. EMMI HA-216 "Extremes of Density and Temperature: Cosmic Matter in the Laboratory". M.G. and T.I.M. acknowledges the support of the FCT, under Contracts No. SFRH/BPD/92455/2013 and SFRH/BPD/69627/2010, respectively. Laboratoire Kastler Brossel is "Unité Mixte de Recherche du CNRS, de l'ENS et de l'UPMC" No. 8552. The authors acknowledge financial support for the experimental determination of FP data by the REXDAB collaboration that was initiated within the International Fundamental Parameter Initiative. J.H. and J.-Cl.D. would also like to thank Dr. T. Huthwelker and the crew of the PSI/SLS beamline PHOENIX for the preparation of the synchrotron radiation beam employed for the linewidth measurements.

TABLE V. L subshell fluorescence yield values for Ge.

	ω_{L_1}	ω_{L_2}	ω_{L_3}
This work (Theo.)	1.49×10^{-3}	1.51×10^{-2}	1.36×10^{-2}
This work (Expt.)			$1.20(11) \times 10^{-2}$
Puri <i>et al.</i> (RDHS) (1993) [43]	1.05×10^{-3}	1.42×10^{-2}	1.36×10^{-2}
McGuire (1971) [46]	7.70×10^{-4}		1.44×10^{-2}
Chen <i>et al.</i> (1971) [47]		7.72×10^{-3}	
Krause (1979) [45]	2.40×10^{-3}	1.30×10^{-2}	1.50×10^{-2}

- [1] D. Coster and R. D. L. Kronig, *Physica* **2**, 13 (1935).
- [2] R. Jenkins, R. Manne, R. Robin, and C. Senemaud, *X Ray Spectrom.* **20**, 149 (1991).
- [3] G. H. Zschornack, *Handbook of X-Ray Data* (Springer, 2007).
- [4] R. W. Fink, R. C. Jopson, H. Mark, and C. D. Swift, *Rev. Mod. Phys.* **38**, 513 (1966).
- [5] E. J. McGuire, *Phys. Rev. A* **2**, 273 (1970).
- [6] D. L. Walters and C. P. Bhalla, *Phys. Rev. A* **3**, 1919 (1971).
- [7] W. Bambynek, B. Crasemann, R. W. Fink, H. U. Freund, H. Mark, C. D. Swift, R. E. Price, and P. V. Rao, *Rev. Mod. Phys.* **44**, 716 (1972).
- [8] C. P. Bhalla, *J. Phys. B: At. Mol. Phys.* **3**, 916 (1970).
- [9] M. H. Chen, B. Crasemann, and H. Mark, *Phys. Rev. A* **21**, 436 (1980).
- [10] M. H. Chen, B. Crasemann, and H. Mark, *Phys. Rev. A* **24**, 177 (1981).
- [11] M. H. Chen, B. Crasemann, and H. Mark, *Phys. Rev. A* **21**, 449 (1980).
- [12] M. H. Chen, B. Crasemann, and H. Mark, *Phys. Rev. A* **27**, 2989 (1983).
- [13] J. M. Sampaio, T. I. Madeira, J. P. Marques, F. Parente, A. M. Costa, P. Indelicato, J. P. Santos, M. C. Lépy, and Y. Ménesguen, *Phys. Rev. A* **89**, 012512 (2014).
- [14] J. M. Sampaio, F. Parente, P. Indelicato, and J. P. Marques, *J. Phys. B: At. Mol. Opt. Phys.* **46**, 065001 (2013).
- [15] K. Kozio, *J. Quant. Spectrosc. Radiat. Transfer* **149**, 138 (2014).
- [16] B. Beckhoff and G. Ulm, *Adv. X-Ray Anal* **44**, 349 (2001).
- [17] Y. Ménesguen and M. C. Lépy, *Nucl. Instr. Methods B* **268**, 2477 (2010).
- [18] T. L. Hopman, C. M. Heirwegh, J. L. Campbell, M. Krumrey, and F. Scholze, *X Ray Spectrom.* **41**, 164 (2012).
- [19] B. Beckhoff, *J. Anal. At. Spectrom.* **23**, 845 (2008).
- [20] J. P. Desclaux, *Comput. Phys. Commun.* **9**, 31 (1975).
- [21] P. Indelicato and J. Desclaux, *Mcdfgme, a multiconfiguration dirac-fock and general matrix elements program* (2005).
- [22] P. Indelicato, O. Gorveix, and J. P. Desclaux, *J. Phys. B: At. Mol. Phys.* **20**, 651 (1987).
- [23] O. Gorveix, P. Indelicato, and J. P. Desclaux, *J. Phys. B: At. Mol. Phys.* **20**, 639 (1987).
- [24] P. Indelicato, *Nucl. Instr. Methods B* **31**, 14 (1988).
- [25] J. P. Santos, J. P. Marques, F. Parente, E. Lindroth, P. Indelicato, and J. P. Desclaux, *J. Phys. B: At. Mol. Opt. Phys.* **32**, 2089 (1999).
- [26] P. Indelicato and J. P. Desclaux, *Phys. Rev. A* **42**, 5139 (1990).
- [27] P. Indelicato, *Phys. Rev. A* **51**, 1132 (1995).
- [28] P. Indelicato, *Phys. Rev. Lett.* **77**, 3323 (1996).
- [29] P.-O. Löwdin, *Phys. Rev.* **97**, 1474 (1955).
- [30] J. L. Campbell and T. Papp, *At. Data Nucl. Data Tables* **77**, 1 (2001).
- [31] S. T. Perkins, D. E. Cullen, M.-H. Chen, J. H. Hubbell, J. Rathkopf, and J. H. Scofield, *Lawrence Livermore National Laboratory Report UCRL-50400* **30** (1991).
- [32] R. D. Deslattes, E. G. Kessler, P. Indelicato, L. de Billy, E. Lindroth, and J. Anton, *Rev. Mod. Phys.* **75**, 35 (2003).
- [33] M. Mueller, B. Beckhoff, G. Ulm, and B. Kanngießner, *Phys. Rev. A* **74**, 012702 (2006).
- [34] B. Beckhoff and G. Ulm, *Determination of fluorescence yields using monochromatized undulator radiation of high spectral purity and well-known flux*, vol. 44 (*Adv. X-Ray Anal.*, 2001).
- [35] P. Hönicke, M. Kolbe, M. Müller, M. Mantler, M. Krämer, and B. Beckhoff, *Phys. Rev. Lett.* **113**, 163001 (2014).
- [36] M. Kolbe, P. Hönicke, M. Müller, and B. Beckhoff, *Phys. Rev. A* **86**, 042512 (2012).
- [37] B. Beckhoff, A. Gottwald, R. Klein, M. Krumrey, R. Muller, M. Richter, F. Scholze, R. Thornagel, and G. Ulm, *Phys. Status Solidi B* **246**, 1415 (2009).
- [38] A. Gottwald, U. Kroth, M. Krumrey, M. Richter, F. Scholze, and G. Ulm, *Metrologia* **43**, S125 (2006).
- [39] F. Scholze and M. Procop, *X Ray Spectrom.* **30**, 69 (2001).
- [40] M. Muller, B. Beckhoff, R. Fliegau, and B. Kanngiesser, *Phys. Rev. A* **79**, 032503 (2009).
- [41] J. Hozzowska, J.-C. Dousse, J. Kern, and C. Rhme, *Nuclear Instruments and Methods in Physics Research Section A: Accelerators, Spectrometers, Detectors and Associated Equipment* **376**, 129 (1996), ISSN 0168-9002.
- [42] R. Deslattes, E. Kessler, P. Indelicato, L. de Billy, E. Lindroth, and J. Anton, *Rev. Mod. Phys.* **75**, 35 (2003).
- [43] S. Puri, D. Mehta, B. Chand, N. Singh, and P. N. Trehan, *X Ray Spectrom.* **22**, 358 (1993).
- [44] J. L. Campbell, *At. Data Nucl. Data Tables* **85**, 291 (2003).
- [45] M. O. Krause, *J. Phys. Chem. Ref. Data* **8**, 307 (1979).
- [46] E. J. McGuire, *Phys. Rev. A* **3**, 587 (1971).
- [47] M. H. Chen, B. Crasemann, and V. O. Kostroun, *Phys. Rev. A* **4**, 1 (1971).